Simulations of the Transformation Stage of the Extratropical Transition of Tropical Cyclones

ELIZABETH A. RITCHIE AND RUSSELL L. ELSBERRY

Department of Meteorology, Naval Postgraduate School, Monterey, California

(Manuscript received 29 December 1999, in final form 16 October 2000)

ABSTRACT

The physical mechanisms associated with the transformation stage of the extratropical transition of a tropical cyclone are simulated with a mesoscale model using initial environmental conditions that approximate the mean circulations defined by Klein et al. The tropical cyclone structural changes simulated by the U.S. Navy Coupled Ocean–Atmosphere Model Prediction System mesoscale model during the three steps of transformation compare well with available observations. During step 1 of transformation when the tropical cyclone is just beginning to interact with the midlatitude baroclinic zone, the main environmental factor that affects the tropical cyclone structure appears to be the decreased sea surface temperature. The movement of the tropical cyclone over the lower sea surface temperatures results in reduced surface heat and moisture fluxes, which weakens the core convection and the intensity decreases. During step 2 of transformation, the low-level temperature gradient and vertical wind shear associated with the baroclinic zone begin to affect the tropical cyclone. Main structural changes include the development of cloud-free regions on the west side of the tropical cyclone, and an enhanced ''delta'' rain region to the northwest of the tropical cyclone center. Gradual erosion of the clouds and deep convection in the west through south sectors of the tropical cyclone appear to be from mechanically forced subsidence due to the convergence between the midlatitude flow and the tropical cyclone circulation. Whereas the warm core aloft is advected downstream, the mid- to low-level warm core is enhanced by subsidence into the tropical cyclone center, which implies that the low-level cyclonic circulation may continue to be maintained.

Step 3 of transformation is the logical conclusion of structural changes that were occurring during steps 1 and 2. Even though the tropical cyclone circulation aloft has dissipated, a broad cyclonic circulation is maintained below 500 mb. Although the low-level warm core is reduced from step 2, it is still significantly stronger than at step 1, and a second warm anomaly is simulated in a region of strong subsidence upshear of the tropical cyclone remnants. Whereas some precipitation is associated with the remnants of the northern eyewall and some cloudiness to the north-northeast, the southern semicircle is almost completely clear of clouds and precipitation.

1. Introduction

In the western North Pacific, on average 15 typhoons transform into extratropical storms every year. Although these storms do not have the intense inner-core winds of typhoons, the large extent of asymmetrically distributed gale force winds and precipitation, variability in intensity, and the rapid forward motion of these storms make them a significant forecast challenge (Foley and Hanstrum 1994). Improved understanding of the physical processes associated with extratropical transition is essential to better predict their future impacts.

In general, the extratropical transition of a tropical cyclone has been described in terms of the interaction with the large-scale environment into which it translates (e.g., Matuno and Sekioka 1971; Harr and Elsberry 2000). Many studies (e.g., DiMego and Bosart 1982; Sinclair 1993; Foley and Hanstrum 1994; Bosart and Lackmann 1995; Browning et al. 1998) have demonstrated that considerable variability may exist depending on the nature of both the tropical cyclone and the large-scale environment it is embedded within. In addition, the large-scale environment also has seasonal variability that may produce differences in the physical processes associated with extratropical transition.

Despite this variability, the Klein et al. (2000) study of 30 cases of extratropical transition in the western North Pacific found little or no correlation between the physical characteristics (intensity, size) of the tropical cyclone and the subsequent reintensification as an extratropical cyclone. Furthermore, they noted that satellite imagery depictions of the structure changes of the tropical cyclones as they begin to interact with the midlatitude baroclinic zone were generally similar, regardless of the initial size and intensity of the tropical cyclone. It was only during the reintensification as an extratropical storm that differences from case to case became apparent. Thus Klein et al. (2000) propose a

Corresponding author address: Dr. Elizabeth A. Ritchie, Dept. of Meteorology, Code MR/Ri, Naval Postgraduate School, 589 Dyer Rd., Room 254, Monterey, CA 93943-5114.
E-mail: ritchie@nps.navy.mil

two-stage definition of extratropical transition. During the *transformation* stage, the tropical cyclone structure of a nearly symmetric core convection and rainbands (Fig. 1a) changes into a highly asymmetric cloud pattern (Figs. 1b–d), with the convection concentrated in the northern quadrants of the storm, which is more characteristic of a baroclinic wave. In addition, outflow in the upper troposphere is favored in the northern and northeastern sectors of the storm and the central pressure rises rapidly. If the cyclone enters the *reintensification* stage (rather than just dissipating), the intensification as an extratropical cyclone is via well-known upper-tropospheric dynamical forcing processes dependent primarily on the midlatitude structure.

A conceptual model (Fig. 2) of the transformation stage in the western North Pacific by Klein et al. (2000) describes a three-step progression of the interaction between the tropical cyclone and the midlatitude environment based on satellite imagery and 1° lat × 1° long resolution Navy Operational Global Atmospheric Prediction System (NOGAPS) analyses. Key physical processes during the transformation stage include the interaction of the vortex with a preexisting baroclinic zone that results in advection of cold, dry (warm, moist) air in the west (east) outer quadrants of the tropical cyclone. Klein et al. (2000) attribute the initial development of dry slots in the outer convection in the southwest, and the subsequent extension to the south side of the storm, to the horizontal advection of the cold, dry air (Figs. 1b, 1c, and Fig. 2). In addition, they propose that the advection of tropical air to the east of the storm results in ascent of warm, moist air parcels over the tilted isentropes associated with the baroclinic zone (Figs. 2b, c), which results in the development of a multilayer cloud with embedded deep convection in the northern sector of the storm (Figs. 1c, d). They also hypothesize that other trajectories result in the isentropic descent of unsaturated air into the core of the tropical cyclone in the southern sector of the storm, which eventually leads to an erosion of the deep eyewall convection (Fig. 2b).

Klein et al. (2000) also describe with the 1° lat × 1° long analyses a decay and tilt of the tropical cyclone warm core aloft in response to environmental vertical wind shear associated with the baroclinic zone (Fig. 2c). Strong, westerly winds aloft are proposed to account for a sharp cirrus edge on the upshear side (Figs. 1b, d). Model simulations (e.g., Frank and Ritchie 1999) have shown that the interaction of a tropical cyclone–like vortex with vertical wind shear results in a dipole of vertical motion that will tend to suppress convection in the upshear right (southwest) quadrant. Thus, an alternate hypothesis to that of Klein et al. (2000) is that the eyewall convection may be suppressed due to processes associated with the interaction of the tropical cyclone with the environmental vertical wind shear. Finally, Klein et al. (2000) consider the transformation stage finished when the storm center is embedded in cold, descending air within the baroclinic zone (Fig. 2c).

The striking similarities in the satellite imagery during the transformation stage that Klein et al. (2000) observe in all 30 cases has led to their hypothesis that tropical cyclone transformation processes are essentially the same for every tropical cyclone regardless of initial size and intensity. Thus, it should be possible to represent the primary transformation processes by simulating the interaction between an idealized tropical cyclone and a baroclinic zone using a mesoscale model. Using the three steps of the Klein et al. (2000) conceptual model as a framework to guide model simulations, the physical processes during the transformation stage will be examined in more detail than is possible with satellite imagery and 1° lat × 1° long NOGAPS analyses. Simulations will be discussed that reveal the processes during each step of the Klein et al. conceptual model. The objective is to highlight major processes that may be common to many cases of extratropical transition. Key issues to be examined include the processes that result in the dry slot formation and erosion of the southern eyewall convection, the role of the baroclinic zone in modifying the airflow around the tropical cyclone, and the resulting structure of the cyclone at the end of the transformation stage. In addition to providing high space and time resolution model datasets to study transformation processes, model sensitivity tests allow isolation of features of the large-scale environment that produce different responses in the tropical cyclone structure.

The structure of the paper will be as follows. A description of the modeling system will be provided in section 2. After validating in section 3 certain aspects of the simulated cloud structures relative to the Klein et al. (2000) observations, the simulated transformation processes will be examined in detail. Some inferences from the simulations will be compared with the Klein et al. (2000) interpretations to develop an improved understanding of the physical processes involved in the transformation stage of extratropical transition. Summary and conclusions are provided in section 4.

2. Description of the modeling system

a. Model description

The model employed in the study is the U.S. Navy Coupled Ocean–Atmosphere Model Prediction System (COAMPS) that is described in detail by Hodur (1997). The system is nonhydrostatic, has multiple nested grids, and includes a Kain-Fritsch (KF) representation of convection, explicit moist physics, and boundary-layer processes. An ocean prediction model is not included in this study. The primitive equations are solved on an f plane valid at 20°N, with Cartesian coordinates in the horizontal and a terrain-following σ coordinate in the vertical. The model has 36 layers from $\sigma = 0$ to 1, with the vertical boundaries at 30 km and the surface. Vertical velocity is defined at the interfaces of the model layers,

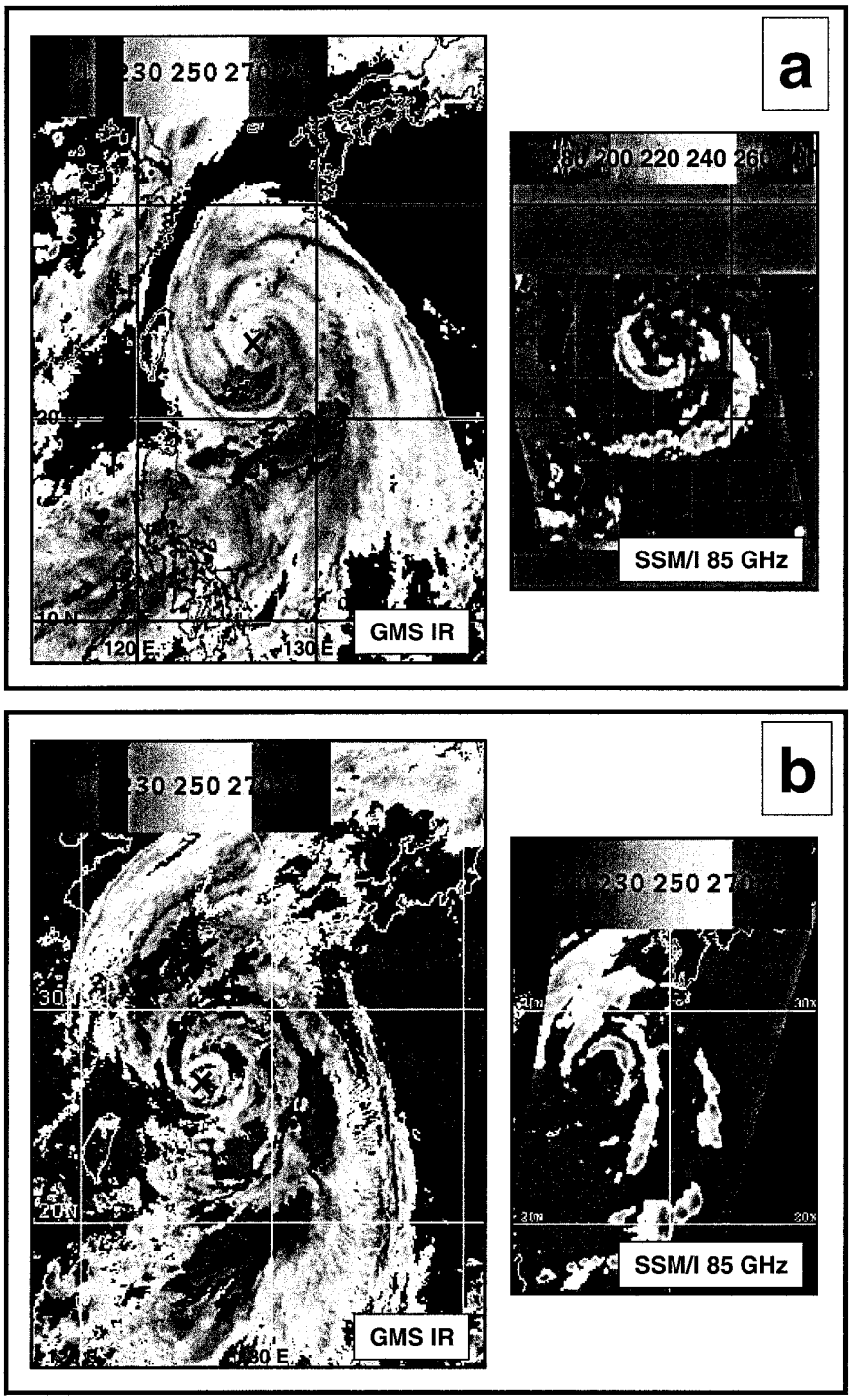

FIG. 1. Satellite infrared and microwave imagery (courtesy of Naval Research Laboratory, Monterey) of Typhoon Peter illustrating the steps of the transformation stage of extratropical transition. A black × indicates the tropical cyclone center: (a) images near 0830 UTC 26 Jun 1997 (pretransformation), (b) images near 0100 UTC 27 Jun 1997 (step 1), (c) images near 1200 UTC 27 Jun 1997 (step 2), (d) images near 1200 UTC 28 Jun 1997 (step 3). The temperature scale for the infrared image in Fig. 1a is approximate. For all other infrared images, dark shades indicate temperatures less than 225 or greater than 270 K.

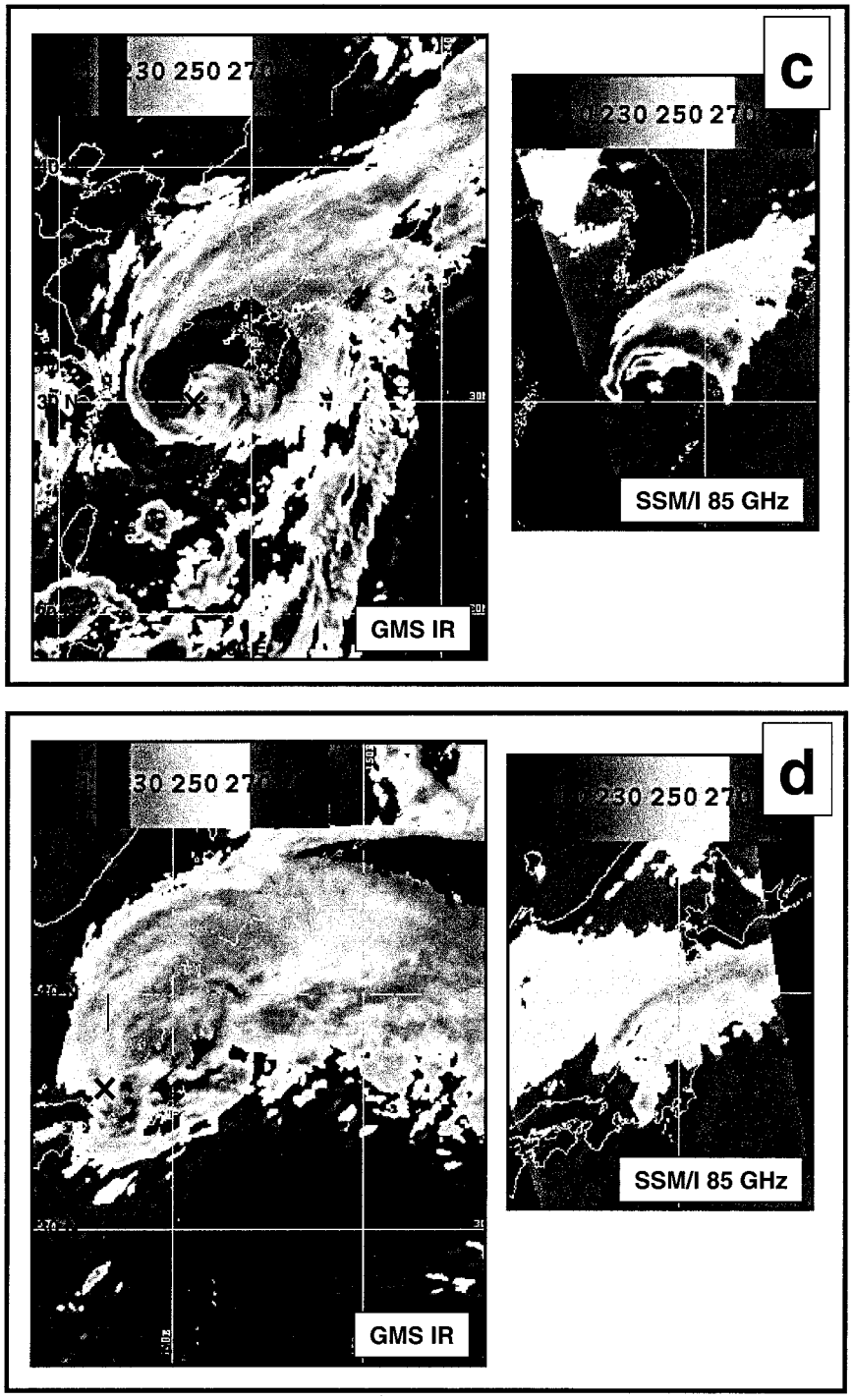

FIG. 1. (*Continued*)

and all other variables are carried at the midpoint of the layers. The horizontal grid has an Arakawa-Lamb C-staggering of the momentum variables (u and v) with respect to the other variables.

In these simulations, the coarse and fine meshes have grid spacings of 45 and 15 km, respectively. The coarse domain of 109 × 85 grid points is large enough to allow an adequate representation of the idealized baroclinic zone during the integration. The fine domain of 151 × 151 grid points captures the primary structural modifications of the storm as it interacts with the baroclinic environment. Only the fine mesh simulations will be presented in the figures. The coarse grid supplies boundary values to the fine mesh, which in turn feeds infor-

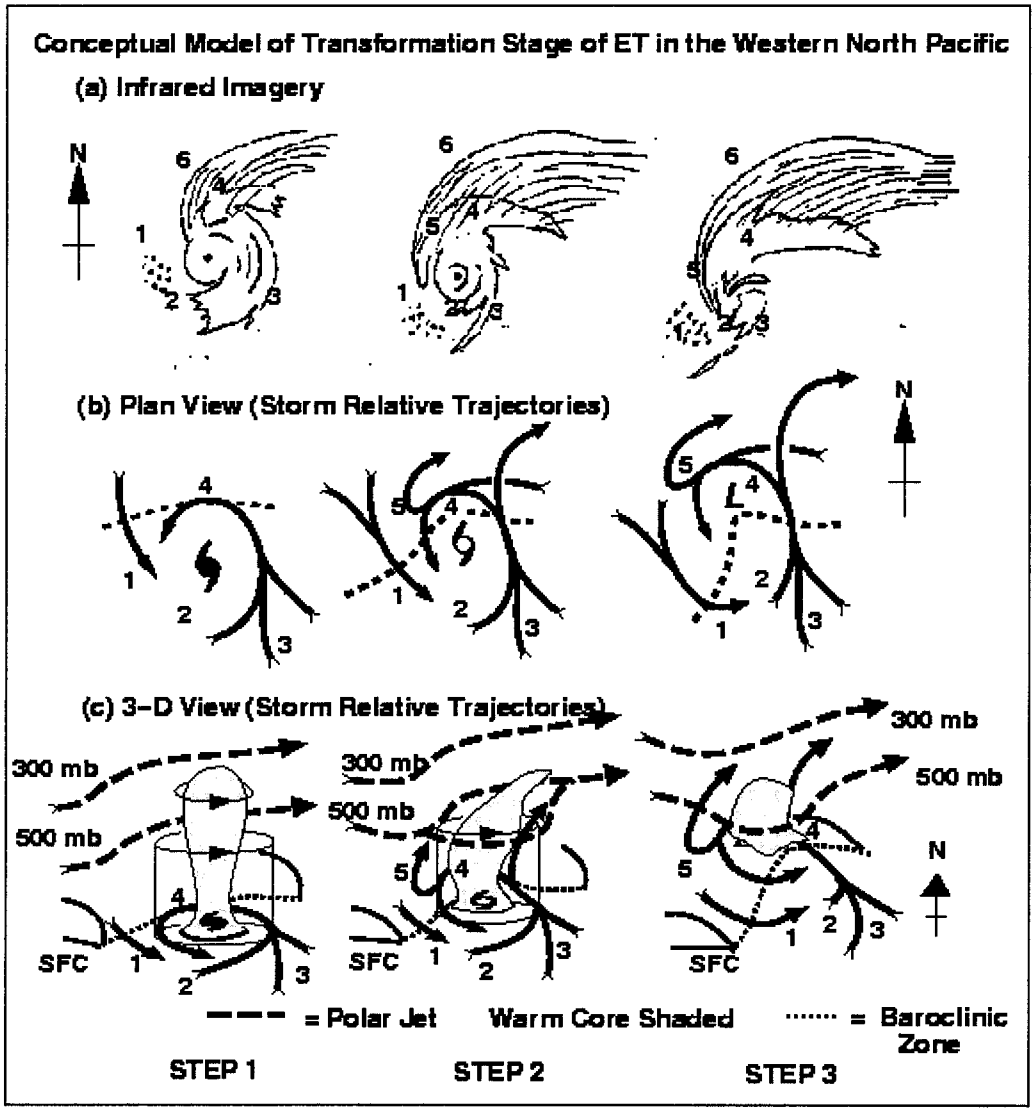

FIG. 2. Schematic by Klein et al. (2000) of the physical processes occurring during the transformation stage of a tropical cyclone: (a) step 1, (b) step 2, (c) step 3.

mation to the coarse grid over the entire fine mesh. Boundary conditions (Perkey and Krietzberg 1976) around the coarse domain force the model-predicted variables near the boundary to adjust to the fixed initial values. The KF scheme (Kain and Fritsch 1993) is employed to treat subgrid-scale convective processes, while the explicit moist physics (Rutledge and Hobbs 1983) treats any grid-scale saturation. Additional parameterizations include subgrid-scale mixing (Deardorff 1980), surface fluxes (Louis 1979), and radiation (Harshvardhan et al. 1987).

b. Experimental setup

According to Klein et al. (2000), transformation commences as the tropical cyclone translates poleward over lower sea surface temperatures (SST) and the outer circulation begins to impinge on a preexisting midlatitude baroclinic zone. Three major environmental interactions that are likely to be important during transformation are examined with these simulations: (i) response to the low-level temperature gradient associated with the baroclinic zone, (ii) response to the SST gradient, and (iii) interaction with the increasing vertical wind shear associated with the midlatitude synoptic pattern. Although the vertical wind shear is related to baroclinic effects in both the low levels and aloft, one objective of these simulations is to separate the upper-level- and low-level-related processes during transformation. No attempt is made to represent all of the midlatitude circulation variability in these simulations. Instead, the intent is to examine the basic processes by specifying somewhat

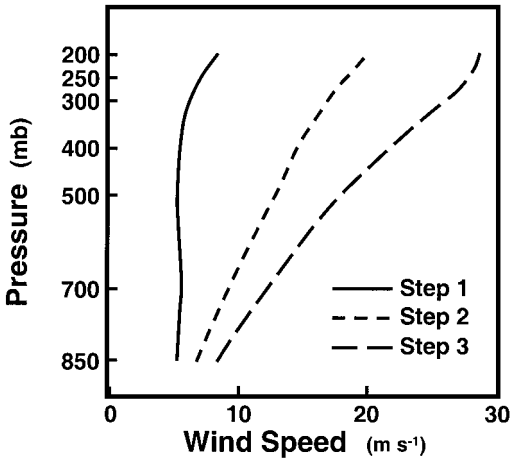

FIG. 3. Vertical structure averaged over 30 transformation cases of the environmental winds azimuthally averaged around the tropical cyclone center at a radius of 600 km (provided by P. Klein).

idealized circulations based on the Klein et al. (2000) study.

Three distinct wind environments are described by Klein et al. (2000) during steps 1–3 of the transformation stage. During step 1, the tropical cyclone has moved northward into a region of lower SSTs, and has approached a cooler, drier atmosphere associated with the midlatitude baroclinic zone. Based on vertical profiles of the azimuthally averaged winds (Fig. 3) during step 1 using 30 cases, the composite extratropical transition environmental wind structure begins with approximately 4 m s^{-1} uniform southwesterly flow up to 400 mb, and then increases to 8.5 m s^{-1} at 200 mb. This upper-level vertical wind shear is associated with the structure of the subtropical ridge, which tilts southward at higher elevations. By step 2 of the transformation, the tropical cyclone is farther north in the subtropical ridge with an increasingly westerly wind regime (Fig. 3). The mean wind profile has southwesterlies of 5 m s^{-1} at 850 mb with an increase to 20 m s^{-1} by 200 mb. For step 3 (Fig. 3), the mean wind is southwesterly at 8 m s^{-1} at 850 mb with an increase to 28 m s^{-1} by 200 mb. Whereas very little directional change ($<7°$) is found in the composite vertical wind shear environments at any stage of transformation, it is noted that some individual cases have more directional change. However, it is assumed that the effects due to environmental directional shear (and thus temperature advection) occur during the reintensification stage of extratropical transition and not the transformation stage that is the focus of this study. Thus, the directional change in the environmental wind with height is neglected in these simulations of transformation.

Idealized wind environments are specified with a vertical structure similar to the composite environments for steps 1, 2, and 3 (Fig. 3) and a horizontal variation that is based on a Gaussian distribution (Fig. 4a). Given this wind structure, the mass and temperature fields are in geostrophic and hydrostatic balance, with vertical structure at the tropical cyclone position for each step specified as the composite pretropical depression sounding of McBride and Zehr (1981) (Figs. 4b–d). The same vertical profile of relative humidity (McBride and Zehr 1981) is specified at each point so that the meridional temperature gradient implies moist (dry) air to the south (north). A time-invariant SST gradient is specified to match the near-surface air temperature gradient so that surface fluxes of moisture and heat do not erode the near-surface temperature structure through the simulation (Figs. 4b–d). The SST of 301.65 K, which is the temperature during the spinup of the simulated tropical cyclone, is specified at the center of the tropical cyclone for all three environments so that no initial shock is imposed on the tropical cyclone. A special condition for step 1 is that the SST gradient is oriented 45° to the air temperature gradient rather than parallel so that the tropical cyclone will be advected across lower SSTs (Fig. 4b). Preliminary simulations had demonstrated that a tropical cyclone in the step 1 position relative to the baroclinic zone that was advected almost along the SST isoline had an extremely slow evolution of the symmetrically distributed core convection to an asymmetric distribution. Because of the 45° orientation of the isolines, the resultant reduction in SSTs from 301.65 to 299 K during in step 1 of transformation results in a realistic simulation of the tropical cyclone structural changes. By contrast, simulated tropical cyclones that remained over warm waters ($T = 301.65$ K) in relatively weak environmental vertical wind shear eventually reintensified (Ritchie and Elsberry 1999). Since tropical cyclones are observed to weaken during transformation (Klein et al. 2000), reintensification in association with high SSTs is inconsistent.

In contrast, for steps 2 and 3, the SST gradient is oriented parallel to the near-surface air temperature gradient (Figs. 4a, b) and the tropical cyclone remains over SSTs of ~301 K, which is considerably elevated from that experienced by transforming tropical cyclones in nature. A possible consequence of elevated SSTs is enhanced oceanic fluxes that result in unrealistic deep convection and latent heat release as the primary energy for the vortex. A sensitivity simulation in which a tropical cyclone vortex was spun up over 299 K and then embedded in the same step 2 baroclinic gradient except that the SSTs were 299 K under the vortex resulted in unrealistic and immediate shut down of oceanic fluxes and also deep convection. This may be due to an inability on the part of the model physics to capture the important boundary-layer processes. Observations indicate that many tropical cyclones do maintain convection for some time after they have moved over lower SSTs.

The initial tropical cyclone is spun up in a quiescent environment defined by the McBride and Zehr (1981)

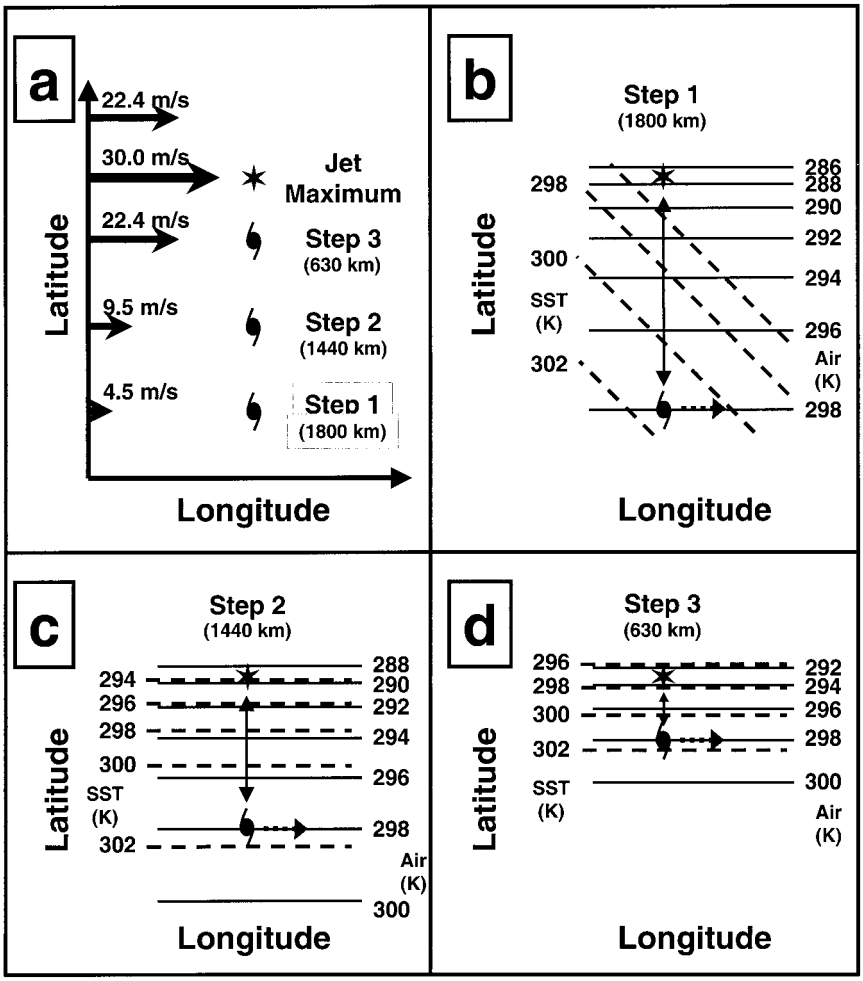

FIG. 4. Idealized representations of the baroclinic environment during the transformation stage. In the three simulations, the tropical cyclone symbols indicate the step 1, 2, and 3 locations relative to the maximum upper-level jet (*) with the horizontal distance from the jet indicated in parentheses: (a) 250-mb wind field indicated by arrows; (b)–(d) horizontal potential temperature contours at 850 mb (solid lines) and SST (dashed lines) for (b) step 1, (c) step 2, and (d) step 3.

composite pretropical depression sounding and constant SST of 301.65 K until an approximately steady-state intensity of 960 mb is reached and the cloud fields are fully developed (Fig. 5a). This initial tropical cyclone has a maximum wind of 55 m s^{-1} at a radius of 70 km (Fig. 5b). The core structure is approximately symmetric with cyclonic winds extending to 50 mb in the core and a maximum T anomaly of 12 K at 450 mb (Fig. 5c). The 300-mb winds turn weakly anticyclonic at 400-km radius. The same initial tropical cyclone wind, temperature, height, and moisture perturbations are added to the environment fields at a location that matches the observed mean environmental wind shear for each step (Fig. 4).

The step 1, 2, and 3 simulations are integrated 48, 24, and 24 h, respectively, either until after the tropical cyclone becomes quasi-balanced with the environment (step 1), or has been completely disrupted. The structures of the simulated tropical cyclone and the environment will be presented at 30, 12, and 18 h, respectively, when the simulated structural changes approximate those of Klein et al. (2000). Although the observed composite wind environment is southwesterly, the idealized environment is specified as westerly for ease of computation. However, the model fields for the step 1, 2, and 3 simulations are rotated 45°, 45°, and 23° anticlockwise, respectively, during postprocessing to compare properly with the environment associated with Typhoon Peter.

c. Typhoon Peter (1997)

Although the simulations were not designed to emulate any one case, the distinct features of transformation that are apparent in satellite imagery for Typhoon Peter are compared with the simulated fields. Typhoon

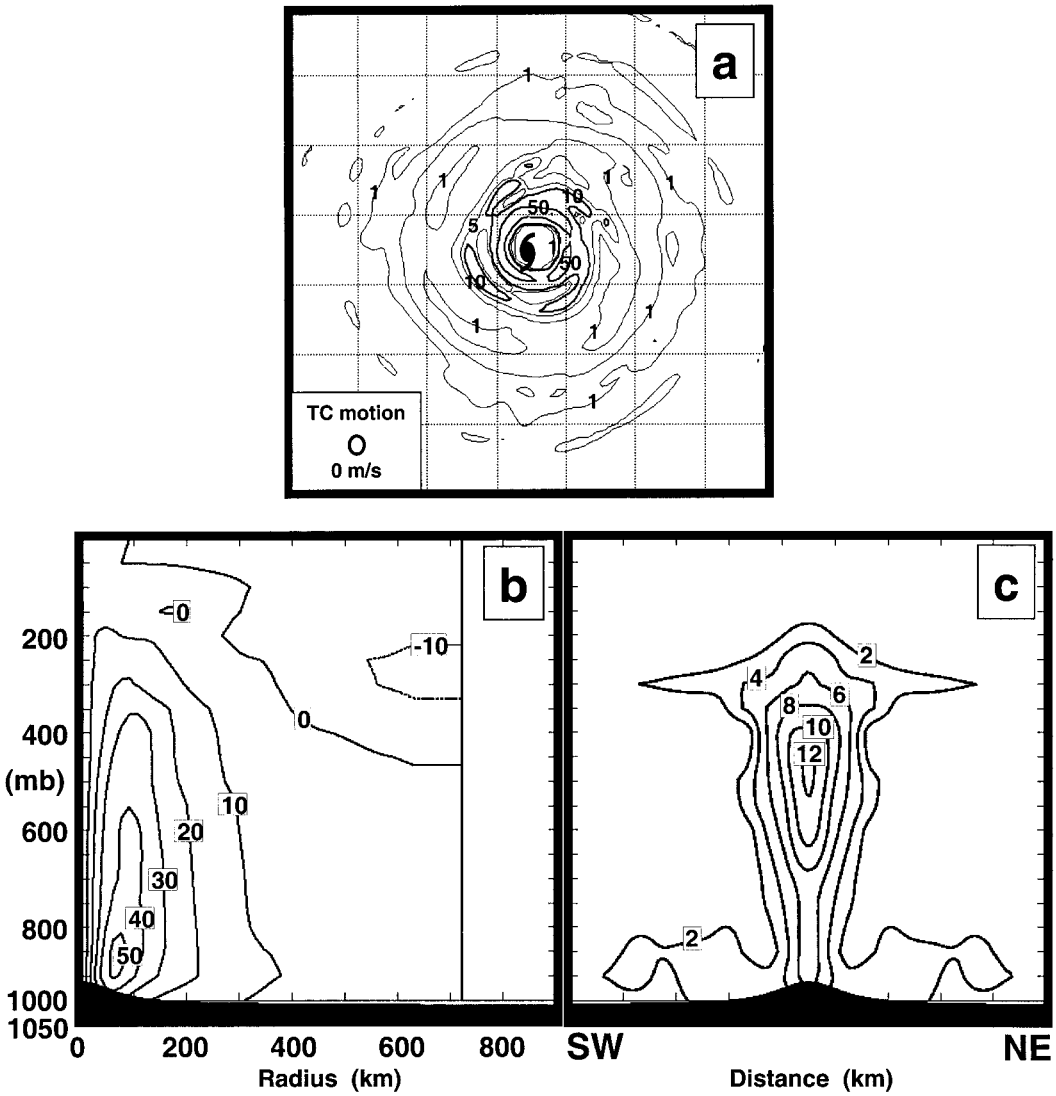

FIG. 5. Simulated pretransformation tropical cyclone fields: (a) pseudocloud image that corresponds to the column-integrated snow and ice mixing ratio (kg kg^{-1}). The grid interval is 2° lat × 2° long. Contour levels are 1, 5, 10, 50, 100, 150 m kg kg^{-1}; (b) azimuthally averaged tangential winds (m s^{-1}); (c) west-east cross section of temperature anomaly (K). Horizontal tick marks are every 100 km.

Peter developed out of a weather disturbance at the eastern end of the monsoon around 20 June 1997. It initially tracked west-northwest as it gradually intensified. On 24 June the then minimal tropical storm began to track northward—a track it maintained for the next 2 days as it intensified to a maximum intensity of 33 m s^{-1} (minimal typhoon) near 0600 UTC 26 June (e.g., Fig. 1a). At about 0000 UTC 27 June, satellite imagery indicated that Typhoon Peter was beginning to undergo transformation processes (Fig. 1b). Around 1200 UTC 27 June (Fig. 1c), the minimal typhoon recurved to the northeast, increased in speed, and made landfall near Sasebo, Japan. Typhoon Peter then moved parallel to the mountainous spine of Honshu (Fig. ld), and subsequently returned to sea. At 0000 UTC 29 June, the transformed remnants of Peter merged with a frontal system and began to reintensify, eventually becoming one of the most intense extratropical cyclones of the season (ATCR 1997).

Simulations of the transformation of Typhoon Peter have indicated that the main cloud and precipitation region that developed during the passage over Japan was associated with interaction with the midlatitude environment. Some localized precipitation was associated with interaction with the topography. However, idealized experiments that removed the island effect produced precipitation patterns that were similar to the control simulation with topography.

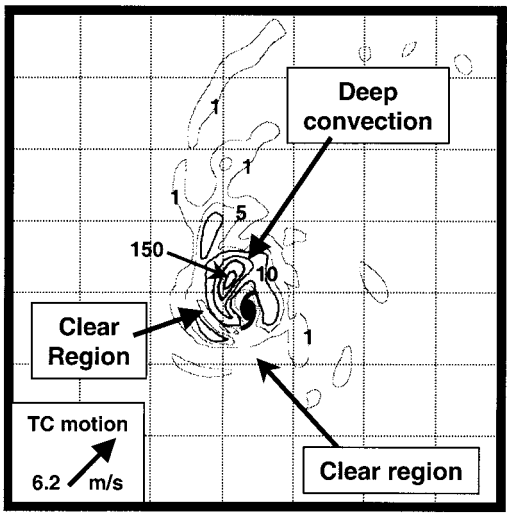

FIG. 6. Simulated step 1 pseudocloud image that corresponds to the column-integrated snow and ice mixing ratio (kg kg^{-1}). The grid interval is 2° lat × 2° long, and the tropical cyclone motion is indicated by the thick black arrow. Contour levels are 1, 5, 10, 50, 100, 150 m kg kg^{-1}.

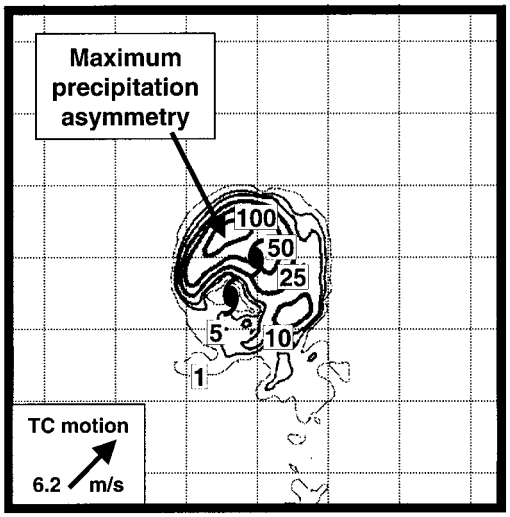

FIG. 7. Simulated step 1 accumulated precipitation (contours = 1, 5, 10, 25, 50, and 100 mm) over 3 h. The grid interval is 1° lat × 1° long, the tropical cyclone motion is indicated by the thick black arrow, and cyclone symbols indicate the positions of the cyclone over the 3 h.

3. Simulations

a. Validation of simulated cloud features during transformation

The simulated changes in the tropical cyclone cloud structure during the transformation are compared both with the individual case of Typhoon Peter and also with the common sequence of satellite imagery described in detail by Klein et al. (2000). Although Typhoon Peter only reached minimal typhoon strength (Fig. 1a) before beginning to transform, many of the characteristic cloud structure changes that occur in transforming tropical cyclones are illustrated in the satellite sequence. The initial tropical cyclone structure is loosely organized with a large rainband that wraps in to a partial eyewall about the west and southern portions of the eye (Fig. 1a). In contrast, the simulated tropical cyclone structure is fairly axisymmetric with four rainbands wrapping into a central, fully circular eyewall (Fig. 5a). These pseudocloud fields are created by calculating the total integrated mixing ratios of ice and snow particles in the column. Values greater than 50 m kg kg^{-1} correspond to very cold temperatures. From satellite imagery, the outer convection (>1.8° lat from the center) in the southwest quadrant of the tropical cyclone has ceased by step 1 of transformation (Fig. 1b. and Fig. 2a), so that the core cloud distribution is becoming more asymmetric. The simulated step 1 cloud fields are qualitatively very similar to the satellite imagery of Typhoon Peter at step 1 (Fig. 1b and Fig. 6). Whereas a cloud-free region in the southwestern quadrant of the simulated tropical cyclone (Fig. 6) matches a similar feature in the satellite imagery (Fig. 1b), deep clouds are located in the southeastern through northwestern quadrants of the simulated tropical cyclone (not shown). A partial eyewall is found in the north through east sectors for both the observed and simulated tropical cyclones at step 1 (Fig. 1b and Fig. 6). The strongest region of convection in the simulated step 1 eyewall is in the northwest quadrant matching the heaviest rainfall (Fig. 7). In addition, weaker convection in the region 2°–5° lat farther out (Fig. 6), is similar to a region in Peter located approximately 5° lat from the center in the northwest quadrant (Fig. 1b), but no precipitation occurs in this outer region (Fig. 7). This is because the pseudo-infrared cloud field is calculated from column-integrated ice and snow and is weighted toward concentration in the upper levels of the atmosphere. However, by comparing the 85-GHz channel of the Special Sensor Microwave Imager (SSM/I) instrument and infrared images in Figs. 1b and 1c, the coldest brightness temperatures in the infrared channels do not always correspond to the deep convection or precipitation indicated by the 85-GHz images and thus are only indicators of where those regions may be. The simulated 3-h precipitation patterns support the thesis that the strongest convection and associated rainfall [convective rainfall defined by precipitation rates >25 mm (3h)$^{-1}$] are occurring in the northwest to north sector of the eyewall (Fig. 7) even at this early stage of transformation.

During steps 2 and 3 of the transformation stage, the observed deep convection continues to decrease so that it has ceased in the southern sector of Peter by step 2 (Fig. 1c) and has no eyewall organization by step 3 (Fig. 1d). The only region of deep convection that is indicated in the 85-GHz imagery by step 3 of transformation is a thin band ~1.5° lat north of the center of Peter (Fig. 1d). The cloud-free region in the southwest quadrant of

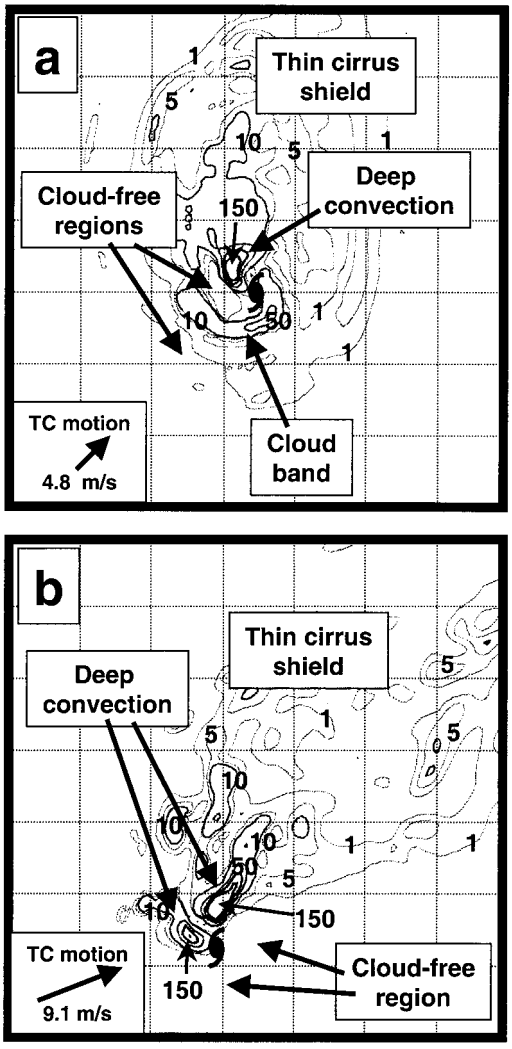

FIG. 8. Simulated pseudocloud images that correspond to the column-integrated snow and ice mixing ratio (kg kg^{-1}) for: (a) step 2 and (b) step 3. The grid interval is 2° lat × 2° long, and the tropical cyclone motion is indicated by the thick black arrow. Contour levels are 1, 5, 10, 50, 100, 150 m kg kg^{-1}.

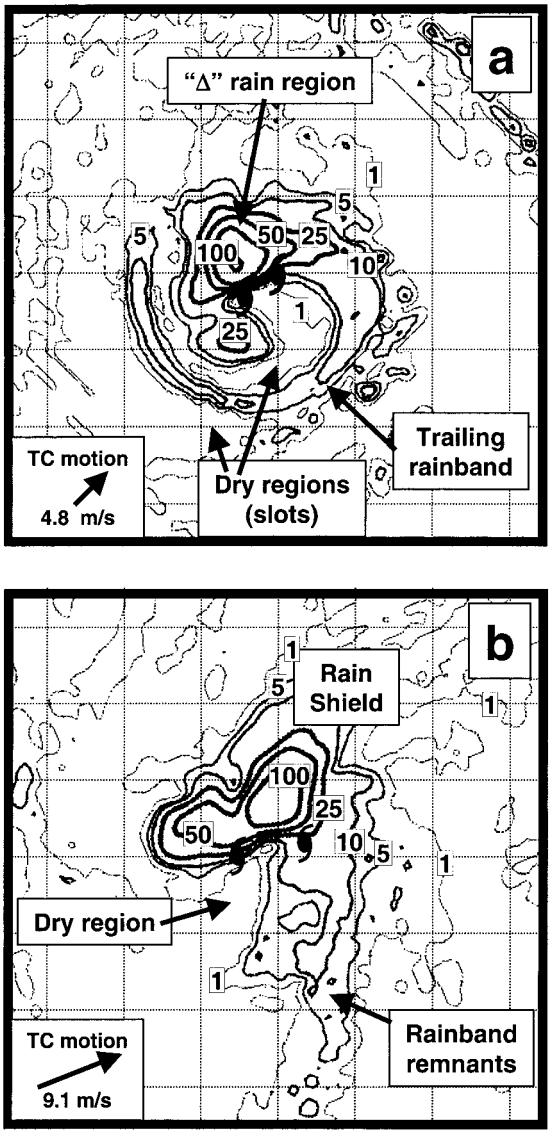

FIG. 9. Simulated precipitation (contours = 1, 5, 10, 25, 50, 100, and 250 mm) accumulated over 3 h for: (a) step 2 and (b) step 3. The grid interval is 1° lat × 1° long, the tropical cyclone motion is indicated by the thick black arrow, and cyclone symbols indicate the positions of the cyclone over the 3 h.

the simulated tropical cyclone also continues to expand during step 2 (Fig. 8a), and deep convection has ceased in the southern sector by step 3 (Fig. 8b). Two regions of deep convection are simulated at step 3—one within 80 km of the center in the northwest quadrant, and one in a band ~1° lat north of the tropical cyclone center (Fig. 8b). Again, this simulated convection is similar to the 85-GHz imagery for both steps 2 and 3 (Figs. 1c, d). In addition, a region of simulated multilayer cloud (between 4 and 11-km depth) that extends more than 3° lat to the north-northeast during steps 2 and 3 (not shown) compares with a similar cloud feature from satellite imagery (Klein et al. 2000) that extends 5° lat to the northeast (Figs. 1c, 1d).

By step 2, the simulated precipitation pattern (Fig. 9a) has become very asymmetric with a maximum in a triangular region northwest of the storm track, minimum precipitation in a curved slot that extends from northwest of the center cyclonically into the southern tropical cyclone core, and a weak trailing rainband feature to the southeast. The triangular region of maximum precipitation is similar to the ''delta'' rain region identified by Shimazu (1998) in radar imagery as being common in typhoons that are approaching midlatitude frontal zones near Japan, and is generally located in the left-front quadrant with respect to the typhoon track. Stratiform precipitation [<25 mm (3h)$^{-1}$] is developing to the northeast of the tropical cyclone center during step 2 (Fig. 9a), and by step 3 a well-developed rain shield

extends northeast of the simulated tropical cyclone center with the largest rainfall within 2° lat (Fig. 9b). This rainfall distribution is similar to SSM/I 85-GHz imagery particularly during step 2 (Fig. 1c), which also has the largest rain rates to the northeast. By Step 3 (Fig. 1d), the 85-GHz imagery indicates the maximum rain rates are to the north of Peter's center in a thin band that extends southwest to northeast and is possibly associated with the midlatitude front. Although the midlatitude frontal system that Peter later merged with during its reintensification stage is not represented in the model environment, an elongation of the simulated precipitation to the north and northeast in the step 3 simulation that was not present during step 2 may represent the development of this thin band of convection. This later development may also explain why the remnants of a weak trailing rainband from the southeastern quadrant to the south in the step 3 simulation agrees more closely with the step 2 satellite imagery (Fig. 9b and Fig. 1c) than the step 3 imagery.

In conclusion, the simulated cloud features (cloud tops, simulated rain rates, and general structural evolution) appear to be validated by the observations of Klein et al. (2000), except that some features in the satellite imagery for Peter at step 3 are not in the simulated cloud fields. Specifically, the start of an interaction between Peter and the midlatitude frontal system that Peter later merges with during its reintensification is not simulated, because a midlatitude frontal system is not represented by the simple baroclinic zone used in these simulations. In addition, the enhanced oceanic fluxes discussed in section 2b may result in some additional enhancement of the precipitation to the north of the simulated tropical cyclone at step 3 (Fig. 9b). With this caveat in mind, it is justified to investigate the model data fields to examine the processes by which this cloud structure and other aspects of the tropical cyclone and baroclinic environment evolve during the transformation stage.

b. Step 1— Interaction with the SST gradient

During step 1 of the simulation, the interaction with the baroclinic zone is confined to the outer circulation, as the large temperature gradient is still far to the north of the circulation center (Fig. 4b). However, the tropical cyclone is translating over lower SSTs (from 301.65 to 299 K), which results in a substantial decrease in the surface latent and sensible heat fluxes and the overall rain rates (Figs. 10a–c) compared with the pretransformation tropical cyclone. Predictably, this results in a weakening of the inner-core convection and thus also the intensity of the vortex (Fig. 10d). Whereas the tropical cyclone inner-core relative vorticity ($>150 \times 10^{-5}$ s^{-1}) is decreased, the surrounding weaker vorticity envelope ($\geq 50 \times 10^{-5}$ s^{-1}) is maintained throughout the step 1 simulation (not shown). Although the maximum tangential winds have decreased, the radius of maximum

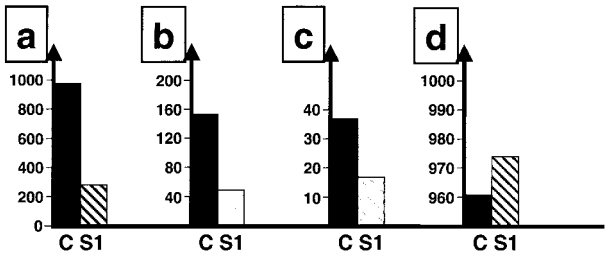

FIG. 10. Surface parameters averaged within 1.5° latitude radius of the simulated tropical cyclone center for the pretransformation vortex (C, solid bars) and step 1 vortex (S1, hatched bars): (a) latent heat flux (W m^{-2}), (b) sensible heat flux (W m^{-2}), (c) 3-h precipitation (mm), and (d) minimum central pressure (mb).

winds (~70 km) has not changed and the outer envelope winds (≥ 10 m s^{-1}) have only broadened from a radius of 390 to 450 km (Fig. 11a and Fig. 5b). Anticyclonic flow aloft has also decreased as expected. The height of the strongest temperature anomaly increases (Fig. 11b and Fig. 5c) and the warm core is eroded by 3°C, which is consistent with a rise in the surface central pressure.

In addition, weak upper-level winds begin to impinge on the tropical cyclone circulation. During this step, the vertical wind shear (Fig. 3) is too weak to disrupt significantly the upper-level tropical cyclone structure. However, an asymmetry does develop in the simulated precipitation (Fig. 7) with larger rain rates in the northeast (front) to northwest (left) quadrants. The maximum precipitation in the northeast quadrant is most likely associated with boundary-layer convergence due to the translation (6.2 m s^{-1}) of the tropical cyclone (Shapiro 1983). However, the primary precipitation maximum, which is in the northwest quadrant, is consistent with both boundary-layer convergence, which tends to be maximum in the front quadrants of a translating tropical cyclone (Shapiro 1983), and also with a vortex tilt explanation based on previous simulations on tropical cyclones in weak vertical wind shear (e.g., Frank and Ritchie 1999). As long as the vortex tilt is less than the radius of maximum winds, the intensity of the tropical cyclone is not likely to be adversely affected by this physical process and the resulting precipitation asymmetry. The beginning of downshear temperature advection above 300 mb (not shown) is also probably due to the weak environmental vertical wind shear.

Thus, the interaction with the lower SSTs is considered to be the most important aspect of the step 1 transformation processes. At least in this step 1 simulation, the inner-core changes in structure arise more from an in situ decrease in convection in response to a lower SST rather than to external influences from either the weak environmental vertical wind shear or the still-distant midlatitude baroclinic zone. Differences will arise with either early or late-season storms as the SST gradient shifts somewhat relative to the upper-level jet. Late-season storms are more likely to be impacted by

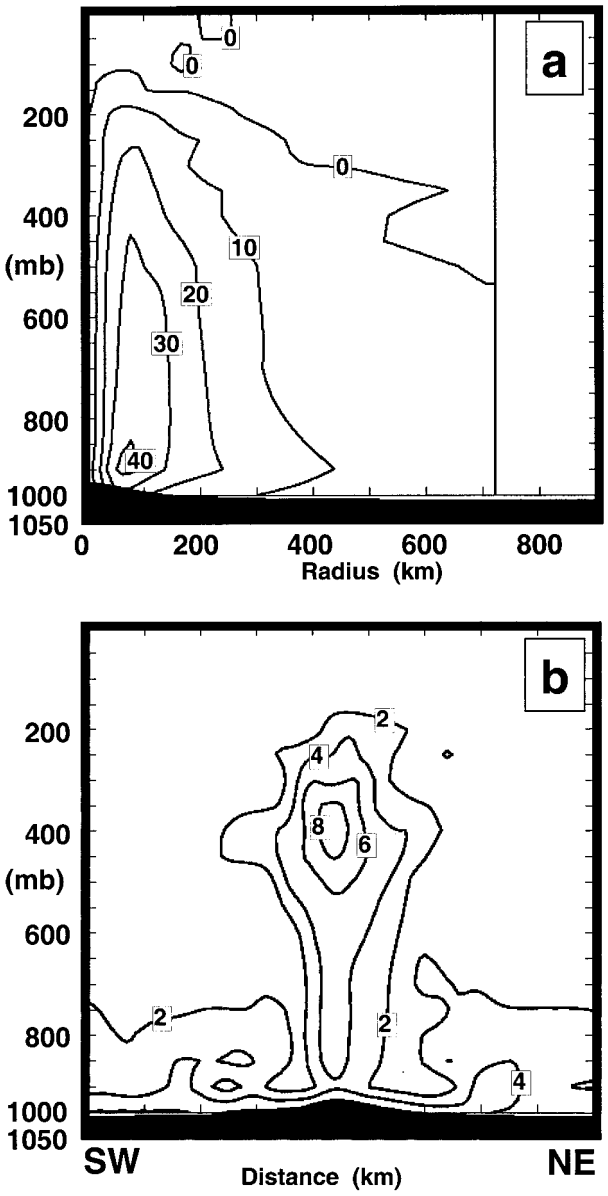

FIG. 11. Simulated step 1 vortex: (a) azimuthally averaged tangential wind field (10 m s^{-1}), and (b) southwest to northeast vertical cross section of temperature anomaly (2 K) along the shear vector. Horizontal tick marks are every 100 km.

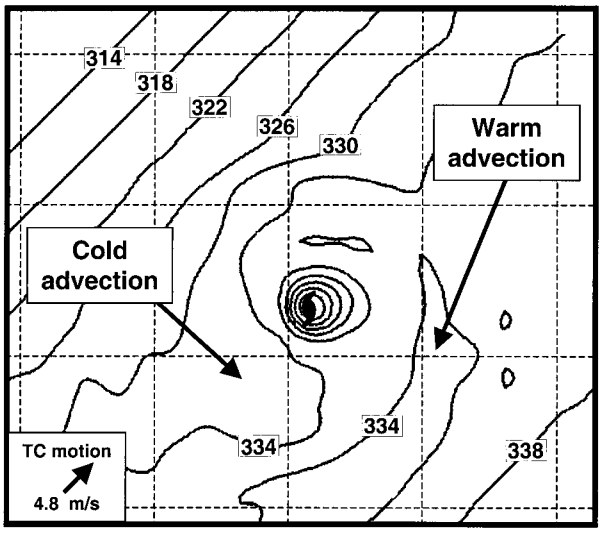

FIG. 12. Equivalent potential temperature (4 K) at 850 mb for the step 2 simulation. The grid interval is 5° lat × 5° long, and the tropical cyclone motion is indicated by the thick black arrow.

stronger environmental vertical wind shear at the same time as moving over lower SSTs.

c. Step 2—Intermediate tropical cyclone structural changes

For the step 2 simulation, the same initial tropical cyclone is placed closer to the baroclinic zone (Fig. 4c), and the relative importance of the environmental influences changes. The interaction between the tropical cyclone outer circulation and baroclinic zone results in the advection of lower θ_e environmental air equatorward around the west side of the tropical cyclone (Fig. 12). Interestingly, it is the lower mixing ratio rather than the lower temperature that accounts for the lower θ_e values. In fact, the 850-mb temperature increases 2 K around the west side of the tropical cyclone because of subsidence warming as the air travels down the sloping isentropes. Klein et al. (2000) linked open-cell cumulus that are commonly associated with heating and moistening of cooler air by surface fluxes from the relatively warmer ocean with advection of cooler air that originated poleward of the baroclinic zone. Relatively enhanced surface fluxes are simulated in the western region of the tropical cyclone compared with the east side (Fig. 13) although the magnitudes are probably elevated because of the elevated SSTs. However, the model physical parameterizations are not able to simulate the open-cell cumulus clouds. On the east side of the tropical cyclone, warm, moist air is advected northward by the outer circulation winds (Fig. 12). Klein et al. (2000) hypothesize that this poleward-flowing air turns cyclonically and begins to interact with the preexisting baroclinic zone with weak ascent over tilted isentropic surfaces.

In contrast to step 1 of transformation, larger departures from the tropical cyclone structure begin during the step 2 simulation as a larger environmental vertical wind shear (westerly at 9.5 m s^{-1}) interacts more strongly with the tropical cyclone circulation. A downshear tilt begins to develop in the inner tropical cyclone structure above 600 mb (e.g., Fig. 14a) with maximum tilt above 300 mb where the cyclonic vorticity is decreased relative to the initial vortex (Fig. 11a and Fig. 14b) so that the inertial stability is weaker. The warm core above 300 mb is also somewhat reduced from the step 1 warm core due to downshear advection of the warm core by

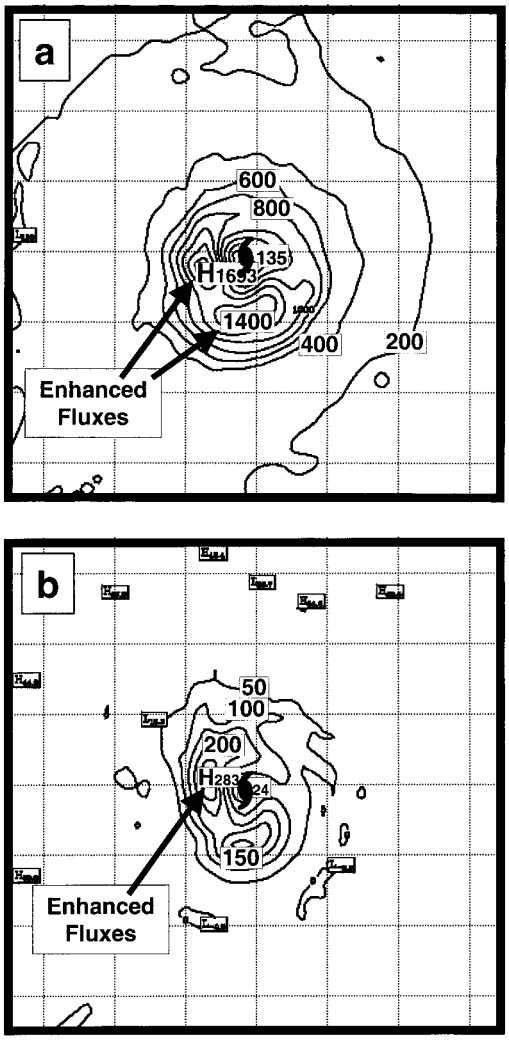

FIG. 13. Surface fluxes for the step 2 simulation: (a) latent heat (200 W m^{-2}) and (b) sensible heat (50 W m^{-2}). The grid interval is 2° lat × 2° long.

the stronger westerlies aloft. Previous simulations (e.g., Bender 1997; Frank and Ritchie 1999) have shown that such a vortex tilt could result in a concentration of convection and precipitation in the front-left quadrant of the tropical cyclone. In this simulation, the front-left quadrant is to the north and northwest of the tropical cyclone center, where the largest precipitation is located in a small triangular-shaped region (Fig. 8a). The translation speed (4.8 m s^{-1}) of the tropical cyclone could also result in frictionally induced boundary-layer convergence (Shapiro 1983) that could enhance convection in the north-to-northeast sectors of the storm. However, little evidence is present that this translation-frictional mechanism is producing the simulated enhanced convection as the strong vertical velocities are concentrated in the northwestern eyewall of the simulated tropical cyclone (Fig. 14c), which is also the location of the strongest surface convergence (not shown).

In contrast to the enhanced vertical velocities being concentrated in the northwestern eyewall, deep mechanically forced subsidence is simulated in the eye and in a band adjacent to the southwest quadrant of the eyewall (Fig. 14d). Since the subsidence in the eye occurs from 200 mb on the inside edge of the southwest eyewall to near the surface and is a maximum near 550 mb, it is the most likely cause of the enhanced warm core near 600 mb (Fig. 14a). This enhancement of the low-level warm core may be the reason that the low-level cyclonic circulation is maintained long after the upper-level warm core has been advected downstream by the strong environmental winds aloft. The downward motion into the eye is associated with convergence in the 200–400 mb layer between the tropical cyclone circulation and midlatitude westerlies (not shown). The weaker band of subsidence just outside the eyewall, also extends from 200 mb to the surface with a maximum downward motion near 800 mb and may be the cause of the second weak warm anomaly (4 K) located upshear of the tropical cyclone center (Fig. 14a). Although the upper-level convergence is the likely cause of the generally subsident region outside the eye, the alternating suppressed convection (cloud-free regions) (Fig. 8a) and precipitation bands (Fig. 9a) in the western through southern sectors of the simulated tropical cyclone (Fig. 14d) may be forced by alternating divergence and convergence in the boundary layer. When the effects of this vertical motion banding structure are combined with that of the low-level stable air that has been advected south from the baroclinic zone (e.g., Fig. 12), the simulated clouds are relatively shallow and generally located in the middle troposphere (not shown).

d. Step 3—Final structure of a transformed tropical cyclone

For the step 3 simulation the same initial tropical cyclone is placed only 630 km from the maximum jet (Figs. 4a, d). Consequently, the interaction between the tropical cyclone outer circulation and baroclinic zone results in stronger advection of colder, drier, environmental air equatorward around the west and south side of the tropical cyclone (Fig. 15), which causes the isentropes to the south of the tropical cyclone to become more tightly packed. A rain-free region more than 3° lat from the tropical cyclone center (Fig. 9b) is colocated with the region of lowest θ_e air (Fig. 15), and may be caused by the gradual isentropic descent of the drier, colder midlatitude air. This is supported by the presence of an anomalously warm, dry region to the southwest of the tropical cyclone center at 850 mb (not shown) that was most likely produced by adiabatic warming of the cooler midlatitude air as it descended down the isentropes and produced a large stable region. Near the surface, less subsidence of the midlatitude air due to isentropic descent occurs, and so colder, drier air is advected over the warm sea. As in step 2, relatively en-

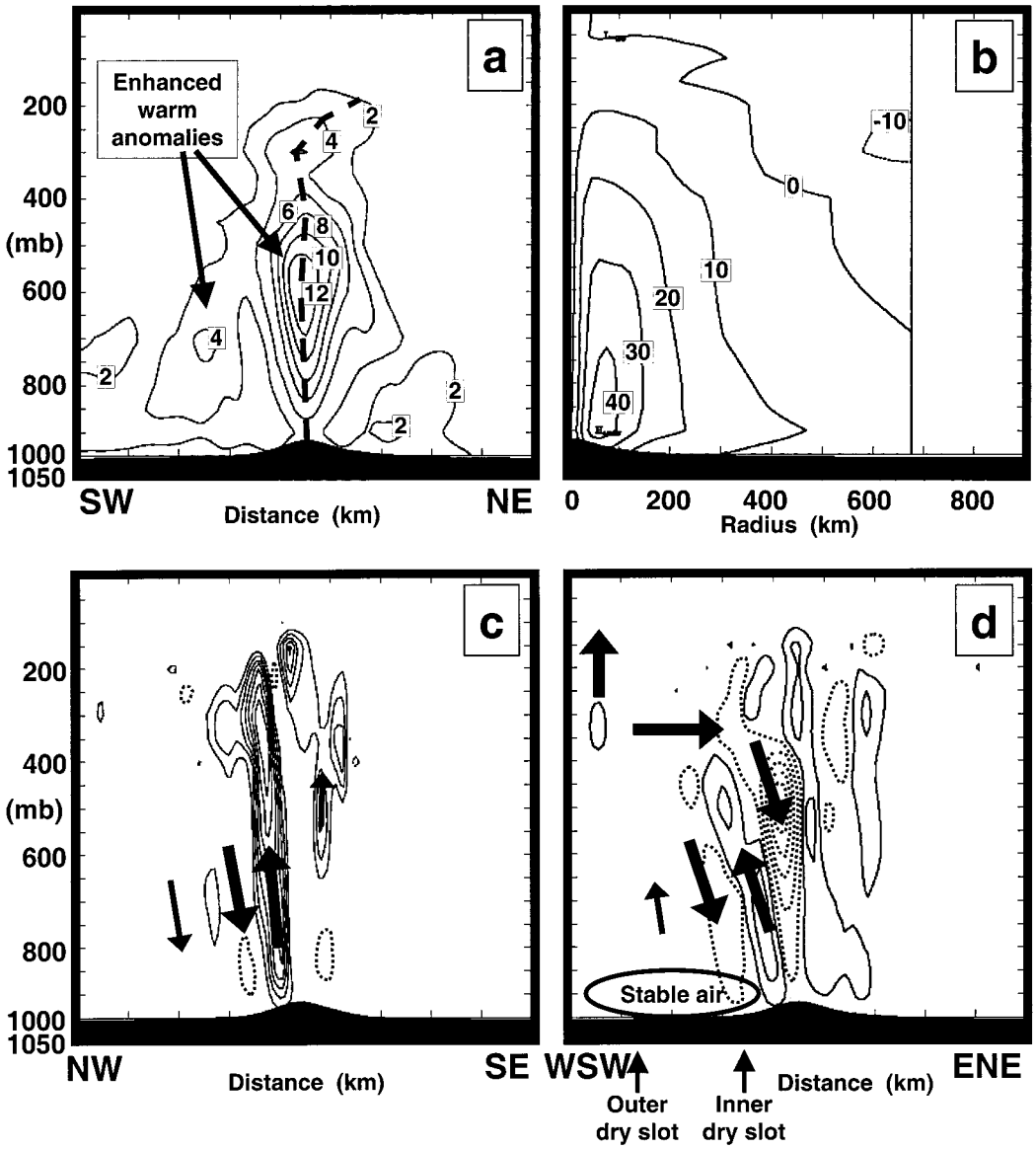

FIG. 14. Step 2 vertical cross sections: (a) temperature anomaly (2 K) in a cross section along the shear vector that is oriented southwest to northeast, (b) azimuthally averaged tangential wind field (10 m s^{-1}), (c) vertical velocity (0.4 m s^{-1}, dashed is negative) in a cross section normal to the shear vector, and (d) vertical velocity (0.4 m s^{-1}, dashed is negative) in a cross section west-southwest to east-northeast. Horizontal tick marks are every 100 km.

hanced surface fluxes are simulated in the northwest through southwest region of the simulated tropical cyclone compared with the east side (Fig. 16).

On the east side of the tropical cyclone, warm, moist air is advected northward by the outer winds, which results in a tightened equivalent potential temperature gradient associated with the midlatitude baroclinic zone (Fig. 15). Poleward-flowing air from the tropical cyclone circulation turns cyclonically as it ascends over tilted isentropic surfaces. Thus, a low-level warm front (not shown) develops on the northern edge of this tropical air. The stratiform [$<$25 mm $(3h)^{-1}$] rain shield in the northeast quadrant of the tropical cyclone during step 3 (Fig. 9b) is consistent with isentropic uplift of the warm, moist air over the cooler midlatitude air associated with the baroclinic zone. The higher rainfall region [$\sim$100 mm $(3h)^{-1}$] just to the northwest of the tropical cyclone center may be a consequence of the enhanced oceanic fluxes forcing deep ascent in that region and is not considered a typical feature of step 3 of a transforming tropical cyclone.

Because the environmental vertical wind shear is stronger in step 3, the initial tropical cyclone structure is even more drastically changed than in step 2 (cf. Fig. 17, Fig. 14). Whereas the cyclonic winds are much reduced above 500 mb, the low-tropospheric cyclonic

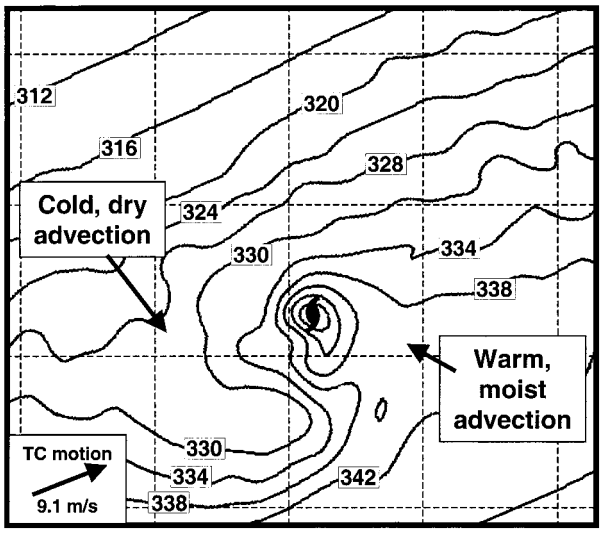

FIG. 15. Equivalent potential temperature (4 K) at 850 mb for the step 3 simulation. The grid interval is 5° lat × 5° long, and the tropical cyclone motion is indicated by the thick black arrow.

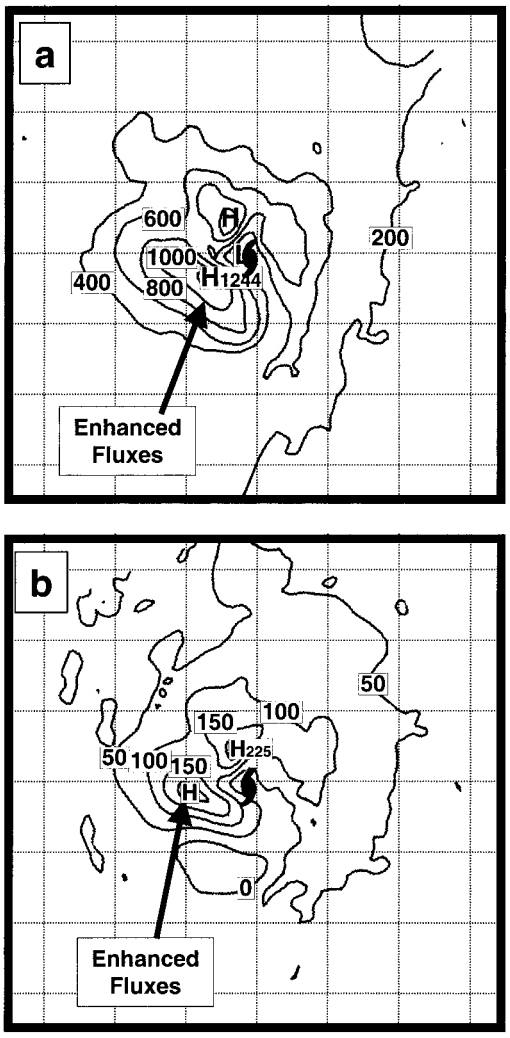

FIG. 16. Surface fluxes for the step 3 simulation: (a) latent heat (200 W m^{-2}) and (b) sensible heat (50 W m^{-2}). The grid interval is 2° lat × 2° long.

wind structure remains coherent (Fig. 17a) even though the maximum wind is decreased to 44 m s^{-1}. A midlevel warm anomaly associated with the remnants of the tropical cyclone warm core remains vertically stacked over the low-level pressure center (thick solid line in Fig. 17b). Some near-surface undercutting of cold, dry air within 50 km of the tropical cyclone center associated with the cold advection on the west side that originated from the preexisting baroclinic zone to the north (Fig. 15) is consistent with the description of Klein et al. (2000), and is one of their criteria for the completion of transformation stage. An additional positive temperature anomaly at 850 mb on the upshear side of the tropical cyclone center extends downward into the cold air to the surface (thin solid line in Fig. 17b) and is strong enough to produce a slight decrease in the surface pressures below. This lower troposphere warm anomaly is consistent with the mechanically forced deep subsidence on the west-southwest side of the tropical cyclone (Fig. 17c) due to convergence between the environmental westerlies and a (shallower) tropical cyclone circulation. Whereas the southwestern convergence in step 2 was concentrated in the upper levels (near 200 mb), the convergence in step 3 is concentrated in the middle levels because the tropical cyclone circulation no longer extends above about 450 mb (Fig. 17a). From tracer analysis, the average residence time of air parcels passing through this subsident region is ~60 min with an average descent of ~1500 m. Thus, adiabatic compression of unsaturated air parcels due to the average decent could theoretically produce a localized warming of ~15 K h^{-1}. Such a large value of warming is not realized locally because of compensating horizontal advection and vertical mixing. However, a maximum low-level warm anomaly of ~9 K is simulated to the west-southwest of the tropical cyclone core coincident with the subsident region. In agreement with subsident warming, the low-level warm anomaly is associated with anomalously dry air (not shown). Vertical mixing of this air with the environmental cold advection from the baroclinic zone may explain why the undercutting of cold air into the cyclone core analyzed by Klein et al. (2000) is not as evident in the simulation (Fig. 17b).

Klein et al. (2000) proposed that the dry sector on the west side of the storm in satellite imagery (e.g., Figs. 1b, c) was due to advection of relatively cool, dry, low-level air from the baroclinic zone into the tropical cyclone circulation. They suggest that the eventual ingestion of this air into the southern portion of the tropical cyclone eyewall may be responsible for the erosion of the southern eyewall (e.g., Fig. 1c). Although the simulated dry region more than 3° lat from the tropical cyclone center may be due to this process, trajectories

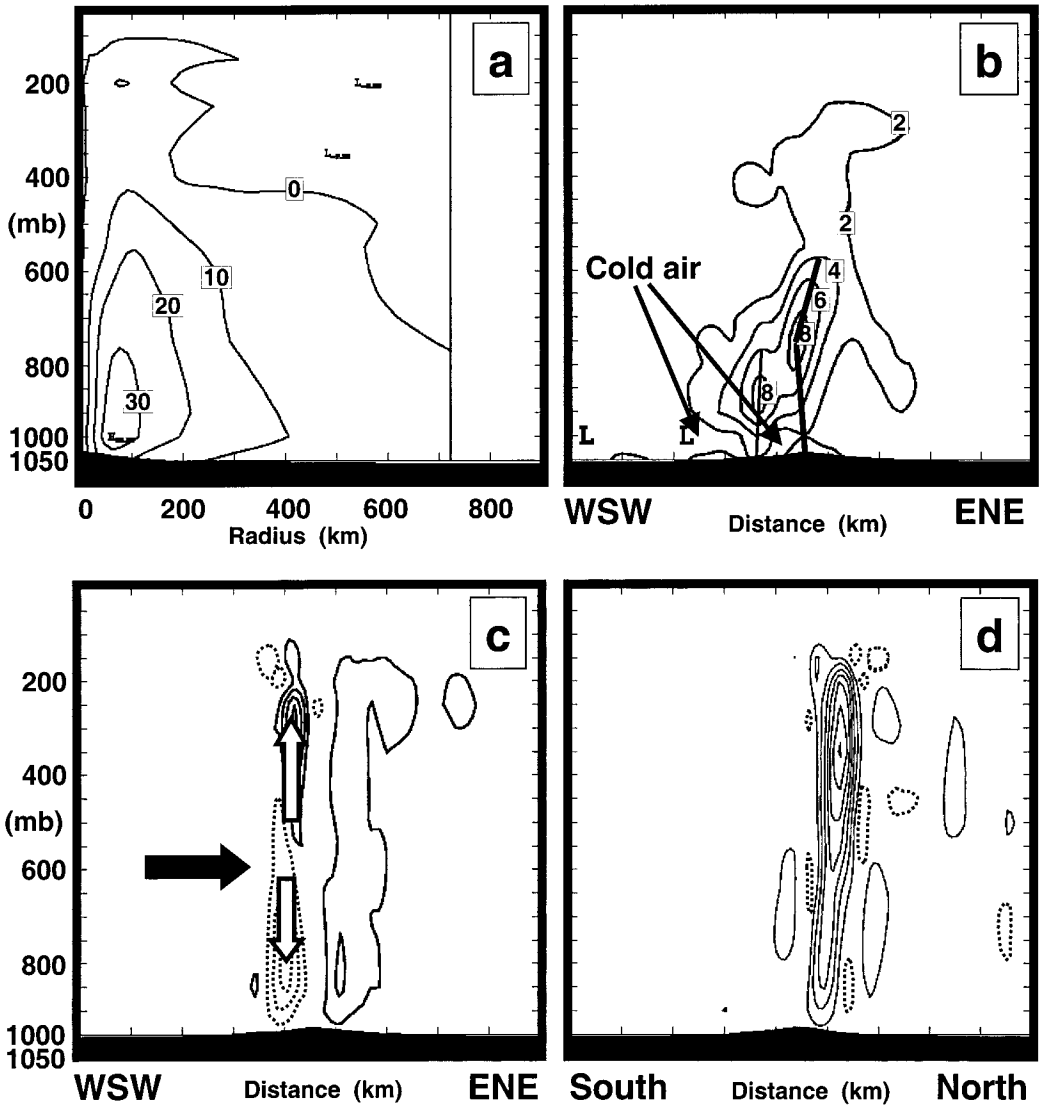

FIG. 17. Simulated step 3: (a) Azimuthally averaged tangential wind field (10 m s^{-1}). Vertical cross sections along a shear vector that is oriented west-southwest to east-northeast for: (b) temperature anomaly (2 K) and (c) vertical velocity (0.4 m s^{-1}, dashed is negative). South to north cross section of (d) vertical velocity (0.8 m s^{-1}, dashed is negative). Horizontal tick marks are every 100 km.

from these simulations do not support ingestion of midlatitude air into the very center of the tropical cyclone. An alternate explanation for the eyewall suppression is supported by these simulations. As a consequence of the deep subsident warming due to the strong convergence at upper levels on the west side of the tropical cyclone just outside the eyewall for step 2 (e.g., Figs. 14a, d) and in the southwest quadrant for step 3 (e.g., Figs. 17b, c), a local stabilization of the atmosphere is simulated in the west through south sectors of the tropical cyclone. Thus, convection and precipitation are completely suppressed in the south within 50 km of the tropical cyclone center (Fig. 9b), which results in the cloud-free region (Fig. 8c). This localized warming mechanism would probably not be resolved by the 1° lat analyses utilized by Klein et al. (2000), which may explain their different conclusion regarding the mechanism leading to suppression of convection in the eyewall.

Whereas the maximum subsidence is simulated on the west side of the step 3 tropical cyclone, the maximum ascent is located to the north of the tropical cyclone center (Fig. 17d). Of particular note is the concentration of the ascent in a thin band extended from north of the center to the northeast. Although, little indication exists either in satellite imagery (Fig. 1d) or in Klein et al.'s conceptual model (Fig. 2) that significant eyewall organization is present by step 3 of transformation, this simulated feature resembles the thin band of colder temperatures in the SSM/I 85-GHz image (Fig.

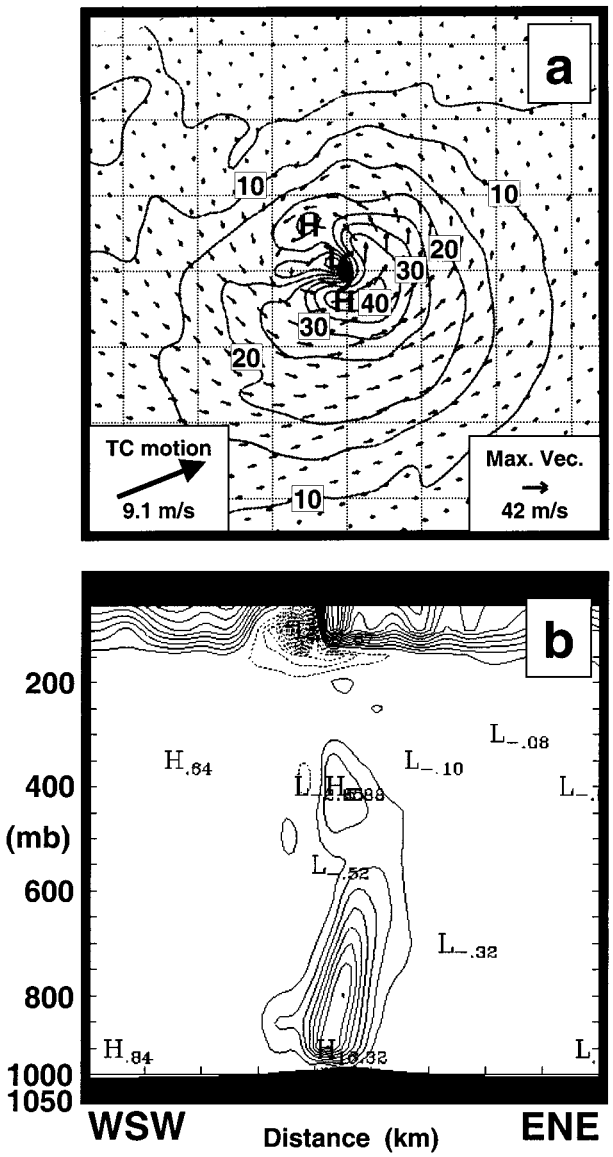

FIG. 18. Simulated step 3: (a) horizontal section of wind speed (m s^{-1}) and vectors at 750 mb, and (b) vertical section of potential vorticity (2 PVU). Horizontal tick marks are every 100 km.

1d—darker gray shades) for Typhoon Peter. Tracer analysis indicates some outer radius ascent due to low-level isentropic uplift within 1400 km from the tropical cyclone center in the northeast sector (not shown), which may be the cause of the multilayer cloud development to the north-northeast of the tropical cyclone center (Fig. 8b) (Schulz and Doswell 1999; Harr and Elsberry 2000).

In addition to the (vertically) reduced, weaker azimuthal circulation (Fig. 17a), the horizontal wind structure at the end of transformation (Fig. 18a) has become highly asymmetric, with stronger (reduced) winds in the right (left) semicircles. Much of the wind asymmetry is due to the large (9.1 m s^{-1}) translation speed of the simulated step 3 tropical cyclone. This simulated wind structure is similar to observations of extratropical transitioning storms in both the Atlantic Ocean (Abraham et al. 1999) and Australian regions (Foley and Hanstrum 1994) where the damaging winds are to the right of track and the heavy precipitation is to the left of track. The outflow associated with the tropical cyclone remnants near 500 mb is similar to that analyzed by Titley and Elsberry (2000) during the decay phase of Supertyphoon Flo (1990). Whereas an environmental flow deflection to the south by the tropical cyclone circulation occurs up to about 450 mb (not shown), little deflection of the environmental flow occurs above that level. Whereas the step 2 potential vorticity profile is deep and vertically stacked with maxima at 800 and 300 mb (not shown), the step 3 maximum potential vorticity is located near the surface and the potential vorticity profile has tilted downshear with height to 600 mb, then upshear to 400 mb (Fig. 18b). In addition, a potential vorticity lobe has developed to the west of the tropical cyclone remnant center (Fig. 18b) that is associated with the secondary low-level warm anomaly and minimum in sea level pressure.

The final transformation stage with a potential vorticity anomaly, and the local equivalent potential temperature maximum in the remnant lower-tropospheric circulation could form the precursor for the reintensification into an extratropical cyclone. This may support the thesis (J. Abraham 1999, personal communication) that particularly damaging extratropical cyclones develop out of transitioning tropical cyclones because of the additional moist, warm air that is associated with the tropical cyclone remnants as it interacts with the midlatitude flow. Implications for reintensification into an extratropical cyclone associated with the development of the secondary dry, positive temperature anomaly and weak sea level pressure perturbation as well as the moist warm air remnants of the simulated tropical cyclone will be explored in future simulations.

4. Summary and conclusions

Using the Klein et al. (2000) three-step transformation conceptual model as a framework, three simulations have been performed that provide a higher time- and spatial-resolution model dataset than the 1° lat × 1° long NOGAPS analyses available to Klein et al. An idealized environment was specified based on composite mean vertical profiles of the azimuthally averaged winds during transformation, and the tropical cyclone was inserted at three appropriate locations relative to the baroclinic zone to represent steps 1, 2 and 3 of the transformation stage. Three major environmental interactions important during transformation have been examined from these simulations with the COAMPS model: (i) response to the low-level temperature gradient associated with the baroclinic zone, (ii) response to the SST gradient, and (iii) interaction with the vertical wind shear associated with the midlatitude synoptic pattern.

Validation of the simulations was accomplished by comparing the simulated cloud fields with satellite imagery of a transforming tropical cyclone. Among the many cloud features that were successfully simulated was the gradual erosion of the clouds in the western quadrant of the tropical cyclone, initially in alternating precipitation bands with cloud-free regions, and finally in a large suppressed region that included the western through southern sectors of the tropical cyclone. Furthermore, a partial eyewall in the northern through eastern sectors was maintained throughout the transformation stage with the strongest ascent in the northern sector of the tropical cyclone. Correspondingly, this was also the location of the strongest precipitation, with a triangular ''delta'' rain region developing during step 2 similar to that observed in radar imagery near Japan. The development of stratiform precipitation [defined by precipitation rates <25 mm $(3h)^{-1}$] similar to a rain shield in the northeast quadrant by step 3 associated with multilayer cloud was also similar to SSM/I and IR satellite imagery of step 3 of a transforming tropical cyclone (e.g., Fig. 1d). Based on these cloud features, it was justified to examine inner-scale feature development that could not be resolved by Klein's dataset and to interpret the simulated physical processes.

In the simulated step 1 of transformation, the tropical cyclone was located far from the baroclinc zone. Thus, the most important environmental interaction was due to the movement of the tropical cyclone over lower SSTs rather than the physical processes that were associated with the midlatitude baroclinic zone. It is unlikely that the weak (4.5 m s^{-1}) vertical wind shear of the step 1 environment would alone produce the structural changes observed by Klein et al. (2000) in satellite imagery. However, the movement of the tropical cyclone over lower SSTs resulted in reduced oceanic fluxes, which weakened the strong axisymmetric core convection and reduced the deep vertical coupling. As the tropical cyclone weakened, there was less resistance to the weak vertical wind shear associated with step 1, and the convection became more asymmetrically distributed. Thus, the movement of the tropical cyclone over lower SSTs is considered important in the transformation process. It is noted that late-season tropical cyclones are more likely to be impacted by stronger vertical wind shear at the same time as moving over lower SSTs.

During step 2 of transformation, the tropical cyclone was placed closer to the baroclinic zone and the relative importance of the environmental influences began to change. The interaction between the low-level tropical cyclone outer circulation with the baroclinic zone resulted in advection of cold, dry (warm, moist) air around the west (east) side of the tropical cyclone. In addition, the upper warm core of the tropical cyclone was diminished in response to environmental vertical wind shear and a slight downshear tilt of the warm core was simulated above 600 mb. This vortex tilt is consistent with other simulations of an asymmetric distribution of the enhanced convection and precipitation associated with the tropical cyclone. In addition, convergence between the upper-level environment winds and the tropical cyclone circulation on the west (upshear) side of the tropical cyclone resulted in strong subsidence into the eye of the simulated tropical cyclone. The subsidence resulted in a substantial increase of the tropical cyclone warm-core anomaly at lower levels. This enhancement of the low-level warm core has implications for the maintenance of the low-level tropical cyclone circulation long after the upper-level warm-core anomaly and circulation have been diminished by the strong midlatitude flow. Additional bands of convergence and associated subsidence outside the western eyewall produced alternating cloud-free regions and precipitation bands.

By step 3, the uplift over isentropes in the northeast quadrant of the tropical cyclone associated with the low-level baroclinic zone hypothesized by Klein et al. (2000) should have been simulated. Whereas some isentropic ascent trajectories were simulated, it has not yet been clarified whether this was the mechanism that produced the multilayer cloud to the northeast of the center. A thorough investigation of isentropic uplift into the northeast of the tropical cyclone, and the corresponding downsloping and ingestion of air into the tropical cyclone core on the west side, will remain for a later study.

In step 3, the vertical shear associated with the environmental wind increased relative to step 2 and the upper-level warm core of the tropical cyclone was simulated to advect downstream. Radical changes to the simulated tropical cyclone structure included a reduction in the height of the tropical cyclone circulation with an outflow layer near 500 mb and enhanced ascent in the north quadrant. The warm anomaly associated with the tropical cyclone remnants was near 750 mb and a second warm anomaly developed upshear of the tropical cyclone core associated with the mechanically forced subsidence between the environment flow and the tropical cyclone circulation. In addition, the southwest quadrant was completely clear of precipitation. It is likely that beyond 200 km from the tropical cyclone center, the clear region is due to a combination of advection of cold, dry air from the midlatitudes as well as stabilization due to subsident warming mid- to upper-level convergence between the tropical cyclone circulation and the environmental flow. However, the environmental air was not simulated to approach within 50 km of the tropical cyclone center, and thus the suppression of the southern eyewall convection is most likely due to the strong forced subsidence. This explanation differs from that proposed by Klein et al. (2000) that the outer cloud erosion and finally eyewall erosion in the western and southern quadrants are due to intrusion of cold, dry air from the baroclinic zone into the inner tropical cyclone core.

In conclusion, many of the physical mechanisms proposed by Klein et al. (2000) to occur during transfor-

mation based on satellite imagery and 1° lat × 1° long resolution NOGAPS analyses were simulated in the higher resolution COAMPS model fields. The most obvious difference between the idealized simulations and the conceptual model is the lack of low-level cold, dry air being ingested in the western quadrant inner core. It was a supposition of Klein et al. (2000) that this ingestion of midlatitude air into the inner circulation and finally into the core of the storm was responsible for the development of the so-called dry slots in the clouds, and then the erosion of the southwest eyewall convection. The modeling results presented here support an alternate hypothesis that subsidence due to convergence between the tropical cyclone upper circulation and the environment flow is more likely the main factor responsible for the cloud-free zones in the southwest quadrant and eventually suppression of the eyewall convection. Future work includes using COAMPS to interpret the physical mechanisms during real-data predictions and to study the processes occurring during the reintensification stage of extratropical transition in an idealized framework.

Acknowledgments. Many aspects of this study were inspired by the research of Dr. P. Harr and P. Klein and has benefited from many discussions with both. The average environment vertical wind profiles that were the basis for the tropical cyclone environment in the simulations of steps 1–3 were kindly provided by P. Klein. Standardization of the satellite imagery that was acquired from different sources was achieved through the expertise of Dr. J. S. Tyo. Numerous comments on an earlier draft by P. Harr and two anonymous reviewers improved the manuscript. The COAMPS model was made available by the Naval Research Laboratory, Monterey, California. This research was sponsored by the Office of Naval Research Marine Meteorology Program.

REFERENCES

Abraham, J., G. Parkes, and P. Bowyer, 1999: The transition of the Saxby Gale into an extratropical storm. Preprints, *23d Conf. on Hurricanes and Tropical Meteorology,* Dallas, TX, American Meteor. Soc., 795–798.

ATCR, 1997: Annual tropical cyclone report U.S. Naval Oceanography Command Center, 227 pp. [Available from Joint Typhoon Warning Center, COMNAVMARIANAS, PSC 489, Box 12, FPO, AP, 96536-0051.]

Bender, M. A., 1997: The effect of relative flow on the asymmetric structure of the interior of hurricanes. *J. Atmos. Sci.,* **54,** 703–724.

Bosart, L. F., and G. M. Lackmann, 1995: Post-landfall tropical cyclone re-intensification in a weakly baroclinic environment: A case study of Hurricane David (September 1979). *Mon. Wea. Rev.,* **123,** 3268–3291.

Browning, K. A., G. Vaughan, and P. Panagi, 1998: Analysis of an extratropical cyclone after its re-intensification as a warm core extratropical cyclone. *Quart. J. Roy. Meteor. Soc.,* **124,** 2329–2356.

Deardorff, J. W., 1980: Stratocumulus-capped mixed layers derived from a three-dimensional model. *Bound.-Layer Meteor.,* **18,** 495–527.

DiMego, M., and L. F. Bosart, 1982: The transformation of tropical storm Agnes into an extratropical cyclone. Part I: The observed fields and vertical motion computations. *Mon. Wea. Rev.,* **110,** 385–411.

Foley, G. R., and B. N. Hanstrum, 1994: The capture of tropical cyclones by cold fronts off the west coast of Australia. *Wea. Forecasting,* **9,** 577–592.

Frank, W. M., and E. A. Ritchie, 1999: Effects of environmental flow upon tropical cyclone structure. *Mon. Wea. Rev.,* **127,** 2044–2061.

Harr, P. A., and R. L. Elsberry, 2000: Extratropical transition of tropical cyclones over the western North Pacific. Part I: Evolution of structural characteristics during the transition process. *Mon. Wea. Rev.,* **128,** 2613–2633.

Harshvardhan, R. Davies, D. Randall, and T. Corsetti, 1987: A fast radiation parameterization for atmospheric circulation models. *J. Geophys. Res.,* **92,** 1009–1015.

Hodur, R. M., 1997: The Naval Research Laboratory's Coupled Ocean/Atmosphere Mesoscale Prediction System (COAMPS). *Mon. Wea. Rev.,* **125,** 1414–1430.

Kain, J., and J. M. Fritsch, 1993: Convective parameterization for mesoscale models: The Kain-Fritsch scheme. *The Representation of Cumulus Convection in Numerical Models, Meteor. Monogr.,* No. 46, Amer. Meteor. Soc., 165–170.

Klein, P. M., P. A. Harr, and R. L. Elsberry, 2000: Extratropical transition of western North Pacific tropical cyclones: An overview and conceptual model of the transformation stage. *Wea. Forecasting,* **15,** 373–395.

Louis, J. F., 1979: A parametric model of vertical eddy fluxes in the atmosphere. *Bound.-Layer Meteor.,* **17,** 187–202.

Matuno, H., and M. Sekioka, 1971: Some aspects of the extratropical transformation of a tropical cyclone. *J. Meteor. Soc. Japan,* **49,** 736–743.

McBride, J. L., and R. M. Zehr, 1981: Observational analysis of tropical cyclone formation. Part II: Comparison of non-developing versus developing systems. *J. Atmos. Sci.,* **38,** 1132–1151.

Perkey, D. J., and C. W. Krietzberg, 1976: A time-dependent lateral boundary scheme for limited-area primitive equation models. *Mon. Wea. Rev.,* **104,** 744–755.

Ritchie, E. A., and R. L. Elsberry, 1999: Mechanisms contributing to extratropical transition of tropical cyclones in the western North Pacific: An idealized study. Preprints, *23d Conf. on Hurricanes and Tropical Meteorology,* Dallas, TX, Amer. Meteor. Soc., 811–814.

Rutledge, S. A., and P. V. Hobbs, 1983: The mesoscale and microscale structure of organization of clouds and precipitation in midlatitude cyclones. VIII: A model for the ''seeder-feeder'' process in warm-frontal rainbands. *J. Atmos. Sci.,* **40,** 1185–1206.

Schultz, D. M., and C. A. Doswell III, 1999: Conceptual models of upper-level frontogenesis in southwesterly and northwesterly flow. *Quart. J. Roy. Met. Soc.,* **125,** 2535–2562.

Shapiro, L. J., 1983: Asymmetric boundary layer flow under a translating hurricane. *J. Atmos. Sci.,* **40,** 1984–1998.

Shimazu, Y., 1998: Classification of precipitation systems in mature and early weakening stages of typhoons around Japan. *J. Meteor. Soc. Japan,* **76,** 437–445.

Sinclair, M. R., 1993: Synoptic-scale diagnosis of the extratropical transition of a southwest Pacific tropical cyclone. *Mon. Wea. Rev.,* **121,** 941–960.

Titley, D., R. L. Elsberry, 2000: Large intensity changes in tropical cyclones: A case study of Supertyphoon Flo during TCM-90. *Mon. Wea. Rev.,* **128,** 3556–3573.